Soft Matter

RSC Publishing

PAPER

View Article Online
View Journal | View Issue

Cite this: *Soft Matter*, 2013, **9**, 9807

Growth modes of condensates on nano-textured surfaces and mechanism of partially wetted droplet formation

Tianqing Liu,* Wei Sun, Xiangqin Li, Xiangyu Sun and Hongru Ai

Condensed droplets on different nano-textured surfaces may appear in three distinct wetting states, the Cassie–Baxter state with composite wetting, Wenzel state with complete wetting, and the partially wetted (PW) state. To maintain the super-hydrophobicity of a textured surface, condensed drops on it are usually expected to be in a Cassie–Baxter or PW state. Therefore, it is of importance to clarify the relation between condensed droplet wetting states and the nano-pillar geometries of surfaces. In view of the fact that all condensed droplets in diverse wetting states originate from the nuclei and/or condensate spots growing along different pathways, we think that the distinct growth modes of a condensate correspond to different energy increasing rates (EIRs), and a condensed drop should grow along the route with the minimum EIR. In this paper, accordingly, the EIRs of a droplet on different textured surfaces were analyzed during its growth along three pathways. The results show that the smallest initial EIR of a condensate spot occurs in the increasing contact angel (CA) mode, so that it will grow with the CA enlarging and the base area initially remaining unchanged. Then the EIR of the increasing CA mode becomes much higher than that of the other two modes. The base area of the drop begins to enlarge while the CA remains unchanged. During this period, the increasing base area can be either in a wetted or composite state, resulting in a Wenzel or PW droplet forming, respectively. The growth mode and the wetting state of a condensed droplet are strongly related to the nano-structure of the surface. Additionally, the calculation results of this model are consistent with experimental observations in the literature for the wetting states of condensed drops on nano-textured surfaces, with an accuracy of 91.9%, which is higher than the accuracy of results calculated with previously reported formulas.

Received 27th June 2013
Accepted 29th August 2013

DOI: 10.1039/c3sm51762d

www.rsc.org/softmatter

1. Introduction

Condensed droplets on different nano-textured surfaces may appear in three distinct wetting states, *i.e.* Cassie–Baxter, Wenzel and partially wetted (PW) state,[1–4] as shown in Fig. 1. Cassie–Baxter drops are formed on the top of nano-pillars so that they suspend on the pillars with the base area in a composite wetting state; the base of a Wenzel droplet is completely wetted; while for a PW drop, only part of its base area is completely wetted while the other region is in a composite state. The wetting state of condensed droplets on nano-textured surfaces seriously impacts the formation rate of the condensate and droplet shedding.

There are several important applications in the power industry, and for air conditioning systems, refrigeration, desalination, water harvesting, self-cleaning of material surfaces, *etc.* that warrant the study of condensation on super-hydrophobic surfaces.[1,2] In all of these applications, condensed droplets are expected to be in a Cassie–Baxter or PW state so that they can leave surfaces as early and quickly as possible.

However, the current experimental results of condensation on various super-hydrophobic surfaces show that almost all micro-textured surfaces lose their super-hydrophobicity under condensation conditions with droplets forming in the Wenzel state.[5–16] It is only on surfaces with suitable nano-structures that condensed droplets can appear in Cassie–Baxter[17–38] or partially wetted (PW) states.[1–4] Meanwhile condensed drops may become

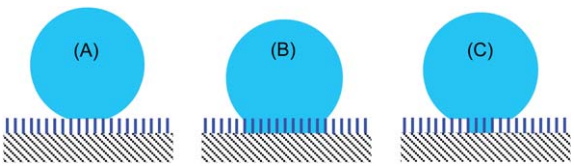

Fig. 1 Three types of droplets on nano-textured surfaces with different wetting states. (A) A Cassie–Baxter droplet suspended on the tops of the pillars. (B) A Wenzel drop with the bottoms of the pillars completely wetted. (C) A partially wetted (PW) droplet with only some of the bottoms of the pillars wetted.

School of Chemical Engineering, Dalian University of Technology, Dalian, 116024, Liaoning Province, P. R. China. E-mail: liutq@dlut.edu.cn

wetted if the nano-textured surfaces are inadequate. Why will condensed drops appear in distinct wetted states on different textured surfaces? *I.e.* why do condensed droplets grow in different wetting modes? And what is the relation between the growth modes of drops and structural parameters? All these issues are waiting to be solved.

The following equation has commonly been used to determine the wetted state of condensed droplets on textured surfaces:[5,6,10,11,18,19]

$$\cos\theta_C = \frac{f-1}{r-f} \quad (1)$$

where f and r are the area fraction of a solid and Wenzel rough factor respectively on a textured surface. A condensed droplet will be in a Cassie–Baxter state when the intrinsic contact angle (CA) θ_I is greater than the critical CA θ_C in this formula, where θ_C corresponds to a minimum energy for a Wenzel or Cassie–Baxter state. Otherwise, the droplet will appear in a Wenzel state. In fact, the physical meaning of this equation is that a droplet in an equilibrium state tends to be in a lower interfacial free energy (IFE) state[6] of either a Cassie–Baxter drop or a Wenzel drop. But condensation is a dynamic process during which condensed drops are usually not in an equilibrium state. It is thus not reasonable to use eqn (1) to judge the wetting state of a condensed droplet.

Enright *et al.*[4] proposed the following energy criterion to determine the wetting state of condensed drops under a non-equilibrium state by replacing the intrinsic CA in eqn (1) with the advancing CA θ_A on a flat surface:

$$E^* = \frac{\cos\theta_A^{CB}}{\cos\theta_A^{W}} = \frac{-1}{r\cos\theta_A} \quad (2)$$

where θ_A^{CB} and θ_A^{W} are the advancing CA for a drop appearing in composite and wetted states respectively on nano-textured surfaces. According to eqn (2), E^* greater than 1 means that the IFE of a composite drop is higher than that of a wetted drop, so that the condensed drop will appear in a wetted state, and *vice versa*. However, this equation may overestimate the wetted state under small supersaturation, namely, even though the condensed droplets on a nano-structured surface appeared in a composite state, the calculated E^* might be greater than 1 in this case.[4] Besides, the physical details of an emerging droplet morphology and evolution process could not be reflected by this equation.[4]

Liu *et al.*[39,40] calculated the IFE of a local condensate while it changed shape from the early spot to a Wenzel or Cassie–Baxter state. The final wetted state of a condensed drop could be determined by the corresponding minimum IFE value. The model however, was based on the assumption that the droplet volume was unchanged during its morphology variation, which does not agree with the updated experimental observations. A recent condensation experiment under environmental scan microscopy showed that a condensed droplet formed in nano-structures grew firstly with its contact angle increasing then with its base area enlarging.[4,30,34,41] That is, the volume of a condensed drop will continue expanding as it grows. Therefore, Liu's model is not applicable for the wetted state calculation of growing droplets.

In short, so far the mechanism is unclear for the growth and wetting modes of condensed droplets on nano-textured surfaces. Why will a condensed drop grow in the mode of initially increasing CA then enlarging base area? Why will the expanded base area of the droplet sometimes be in a wetted state while sometimes in a composite state? What is the quantitative relation between these phenomena and texture parameters? All of these questions need to be studied further.

The formulas to describe the energy increasing rate (EIR) of a condensed drop on nano-textured surfaces during its growth are derived in this paper. The minimum EIR was used as the criterion to determine the modes of growing and wetting of condensed droplets. And the influence of nano-structured parameters on the behavior of condensed drops was also calculated.

2. Physical and mathematical models for the growth of a condensed droplet on nano-textured surfaces

The formation and growth processes of condensed droplets on nano-textured surfaces are shown in Fig. 2. First, the nucleation of condensed micro-droplets occurs within the nano-structures

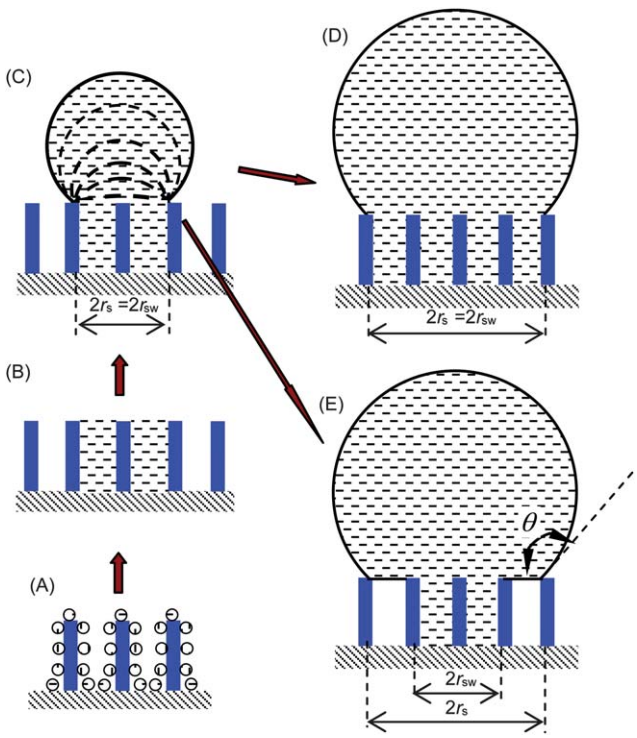

Fig. 2 Schematic of initial condensed droplet formation and growth in nano-structures. The droplet grows in the mode of initially increasing CA then enlarging base area. A completely wetted or a partially wetted droplet will form. (A) Initial nuclei formed amongst the nano-structures. (B) A condensed spot formed by coalescence of growing nuclei. (C) The spot grows up in the mode of increasing CA until a critical CA. (D) The condensed drop continues growing in the mode of enlarging wetted base area. (E) The condensed drop continues growing in the mode of enlarging composite base area.

(Fig. 2A); then, these nucleated droplets coalesce to create a condensate spot (Fig. 2B).[30,34,41] Next, the spot grows in the increasing CA mode[4,30,34,41] (Fig. 2C). Only after the CA reaches a critical value does the base area of the droplet begin to enlarge.[4,30,34,41] And the wetting pattern of the increased base area can be either wetted (Fig. 2D) or composite (Fig. 2E), depending on which process energy barrier is smaller. As shown in Fig. 3, the growth mode of a condensed droplet should be along the pathway with the slowest energy increases or lowest energy barrier. It is thus necessary to calculate and compare the energy variations of a condensed droplet growing in the three different modes respectively, *i.e.* increasing its CA, enlarging its base area with a wetted pattern, and expanding its base area with a composite pattern.

The IFE of a droplet in wetted and PW states and its volume are expressed as:[39,42,43]

$$E_{\mathrm{W}} = \pi\sigma_{\mathrm{LG}}\left[2\frac{{r_{\mathrm{s}}}^2}{\sin^2\theta}(1-\cos\theta) - {r_{\mathrm{s}}}^2\cos\theta_{\mathrm{EW}}\right] + \sigma_{\mathrm{SG}}A_{\mathrm{total}} \quad (3)$$

$$E_{\mathrm{PW}} = \pi\sigma_{\mathrm{LG}}\left[2\frac{{r_{\mathrm{s}}}^2}{\sin^2\theta}(1-\cos\theta) - {r_{\mathrm{sw}}}^2\cos\theta_{\mathrm{EW}} - ({r_{\mathrm{s}}}^2 - {r_{\mathrm{sw}}}^2)\cos\theta_{\mathrm{EC}}\right] + \sigma_{\mathrm{SG}}A_{\mathrm{total}} \quad (4)$$

$$V = \frac{1}{3}\pi{r_{\mathrm{s}}}^3\frac{(2-3\cos\theta+\cos^3\theta)}{\sin^3\theta} \quad (5)$$

where, E_{W} and E_{PW} respectively represent the IFE of a wetted and PW droplet, V is its volume, σ_{LG} and σ_{SG} are the surface and solid–gas interfacial tension respectively, A_{total} is a selected area on the surface, r_{s} and θ are the base radius and apparent CA respectively, r_{sw} is the radius of the wetted part for a PW drop, θ_{EW} and θ_{EC} are the equilibrium CA of wetted and composite droplets respectively. Some of these parameters are shown in Fig. 2.

The changing rates of the IFE and volume of a condensed droplet when it grows in the modes of increasing CA and enlarging base area can be respectively found from the partial derivatives of eqn (3)–(5):

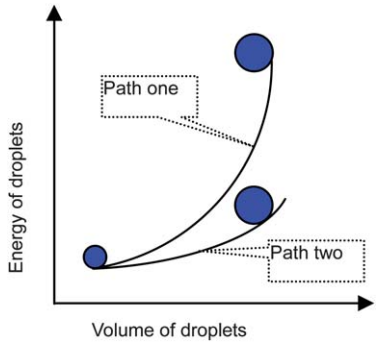

Fig. 3 Schematic of energy increase of droplets with their volume along different pathways. In path one the energy is quickly increasing while in path two the energy is slowly rising. The initial droplet should follow path two in order to grow.

$$\frac{\partial E_{\mathrm{W}}}{\partial\theta} = \frac{\partial E_{\mathrm{PW}}}{\partial\theta} = 2\pi\sigma_{\mathrm{LG}}{r_{\mathrm{s}}}^2\left[-\frac{2\cos\theta}{\sin^3\theta}(1-\cos\theta)+\frac{1}{\sin\theta}\right] = \frac{2\pi\sigma_{\mathrm{LG}}{r_{\mathrm{s}}}^2}{\sin\theta}\left(1-\frac{2\cos\theta}{1+\cos\theta}\right) \quad (6)$$

$$\frac{\partial E_{\mathrm{W}}}{\partial r_{\mathrm{s}}} = 2\pi\sigma_{\mathrm{LG}}r_{\mathrm{s}}\left[\frac{2(1-\cos\theta)}{\sin^2\theta}-\cos\theta_{\mathrm{EW}}\right] = 2\pi\sigma_{\mathrm{LG}}r_{\mathrm{s}}\left(\frac{2}{1+\cos\theta}-\cos\theta_{\mathrm{EW}}\right) \quad (7)$$

$$\frac{\partial E_{\mathrm{PW}}}{\partial r_{\mathrm{s}}} = 2\pi\sigma_{\mathrm{LG}}r_{\mathrm{s}}\left[\frac{2(1-\cos\theta)}{\sin^2\theta}-\cos\theta_{\mathrm{EC}}\right] = 2\pi\sigma_{\mathrm{LG}}r_{\mathrm{s}}\left(\frac{2}{1+\cos\theta}-\cos\theta_{\mathrm{EC}}\right) \quad (8)$$

$$\frac{\partial V}{\partial\theta} = \pi{r_{\mathrm{s}}}^3\frac{\sin^4\theta-\cos\theta(2-3\cos\theta+\cos^3\theta)}{\sin^4\theta} \quad (9)$$

$$\frac{\partial V}{\partial r_{\mathrm{s}}} = \pi{r_{\mathrm{s}}}^2\frac{(2-3\cos\theta+\cos^3\theta)}{\sin^3\theta} \quad (10)$$

Then the changing rates of the IFE of the droplet with its volume increasing by increasing its CA and enlarging its base area can be found from eqn (6) and (9) as well as (7), (8) and (10):

$$\left.\frac{\partial E_{\mathrm{W}}}{\partial V}\right|_{\theta} = \left.\frac{\partial E_{\mathrm{PW}}}{\partial V}\right|_{\theta} = \frac{2\sigma_{\mathrm{LG}}\sin\theta(1-\cos\theta)^2}{r_{\mathrm{s}}[\sin^4\theta-\cos\theta(2-3\cos\theta+\cos^3\theta)]} \quad (11)$$

$$\left.\frac{\partial E_{\mathrm{W}}}{\partial V}\right|_{r_{\mathrm{s}}} = \frac{2\sigma_{\mathrm{LG}}\sin^3\theta}{r_{\mathrm{s}}(2-3\cos\theta+\cos^3\theta)}\left(\frac{2}{1+\cos\theta}-\cos\theta_{\mathrm{EW}}\right) \quad (12)$$

$$\left.\frac{\partial E_{\mathrm{PW}}}{\partial V}\right|_{r_{\mathrm{s}}} = \frac{2\sigma_{\mathrm{LG}}\sin^3\theta}{r_{\mathrm{s}}(2-3\cos\theta+\cos^3\theta)}\left(\frac{2}{1+\cos\theta}-\cos\theta_{\mathrm{EC}}\right) \quad (13)$$

where, $\left.\frac{\partial E_{\mathrm{W}}}{\partial V}\right|_{\theta}$ and $\left.\frac{\partial E_{\mathrm{PW}}}{\partial V}\right|_{\theta}$ respectively represent the changing rates of the IFE of a wetted and PW droplet when their volumes increase through increasing CA, while $\left.\frac{\partial E_{\mathrm{W}}}{\partial V}\right|_{r_{\mathrm{s}}}$ and $\left.\frac{\partial E_{\mathrm{PW}}}{\partial V}\right|_{r_{\mathrm{s}}}$ stand for those when their volumes increase with an enlarging base radius. Although all these changing rates of the IFE result from a volume increase, the pathways of the volume increases are different. One way is through increasing CA, and the other way is through enlarging the base area of the droplet.

The energy increasing rate (EIR) of the droplet considered above is only related to its IFE change as its volume increases. In the case of enlarging the base area of a droplet, the hysteretic force on the three phase contact line (TPCL) needs to be overcome, which results in an energy loss for the drop. Therefore, this energy loss or the work needed must be included when calculating the energy change or energy barrier for the droplet system. The hysteretic force is derived below.

The following relation between CA hysteresis and adhesion work has been well accepted for a Cassie–Baxter or Wenzel drop on a rough surface:[44,45]

$$(\cos\theta_{\mathrm{R}} - \cos\theta_{\mathrm{A}})\sigma_{\mathrm{LG}} = f(1+\cos\theta_{\mathrm{I}})\sigma_{\mathrm{LG}} \quad (14)$$

$$(\cos\theta_R - \cos\theta_A)\sigma_{LG} = r(1 + \cos\theta_I)\sigma_{LG} \quad (15)$$

where θ_R and θ_A are the receding and advancing CA respectively, θ_I is the intrinsic CA. On a flat surface, $f = 1$ and $r = 1$.

Besides, the following formula has been proved:[46]

$$(\cos\theta_R + \cos\theta_A)/2 = \cos\theta_E \quad (16)$$

where the equilibrium CA θ_E becomes θ_{EW} or θ_{EC} respectively for a Wenzel or Cassie–Baxter droplet, which is represented by the Wenzel or Cassie–Baxter equation:

$$\cos\theta_{EW} = r\cos\theta_I \quad (17)$$

$$\cos\theta_{EC} = f\cos\theta_I + f - 1 \quad (18)$$

The following equations can then be derived from the above eqn (14)–(18):

$$(\cos\theta_R - \cos\theta_{EC})\sigma_{LG} = f(1 + \cos\theta_I)\sigma_{LG}/2 \quad (19)$$

$$(\cos\theta_{EC} - \cos\theta_A)\sigma_{LG} = f(1 + \cos\theta_I)\sigma_{LG}/2 \quad (20)$$

$$(\cos\theta_R - \cos\theta_{EW})\sigma_{LG} = r(1 + \cos\theta_I)\sigma_{LG}/2 \quad (21)$$

$$(\cos\theta_{EW} - \cos\theta_A)\sigma_{LG} = r(1 + \cos\theta_I)\sigma_{LG}/2 \quad (22)$$

The physical meaning of eqn (19) and (20) or eqn (21) and (22) is that the driving force (the left of these equations) on the TPCL that is starting to move equals the resistance (the right of these equations) on the TPCL when the apparent CA of the droplet reaches the critical advancing or receding CA. Therefore, the hysteretic force inhibiting the movement of TPCL on textured surfaces can be expressed as the right terms in those equations.

Thus, when the TPCL of a wetted or PW droplet shifts a distance dr_s, the needed work is:

$$dW_W = \pi r(1 + \cos\theta_I)\sigma_{LG} r_s dr_s \quad (23)$$

or

$$dW_{PW} = \pi f(1 + \cos\theta_I)\sigma_{LG} r_s dr_s \quad (24)$$

Accordingly, when a droplet increases its volume by enlarging its base radius, the EIR of droplet system with a volume for wetted and PW droplets, $\left.\frac{\partial E_{SW}}{\partial V}\right|_{r_s}$ and $\left.\frac{\partial E_{SPW}}{\partial V}\right|_{r_s}$, can be found:

$$\left.\frac{\partial E_{SW}}{\partial V}\right|_{r_s} = \left.\frac{\partial E_W}{\partial V}\right|_{r_s} + \frac{dW_W}{dr_s}\Big/\frac{\partial V}{\partial r_s} = \frac{2\sigma_{LG}\sin^3\theta}{r_s(2 - 3\cos\theta + \cos^3\theta)} \times\left(\frac{2}{1+\cos\theta} - \cos\theta_{EW}\right) + \frac{r(1+\cos\theta_I)\sigma_{LG}\sin^3\theta}{r_s(2 - 3\cos\theta + \cos^3\theta)} \quad (25)$$

$$\left.\frac{\partial E_{SPW}}{\partial V}\right|_{r_s} = \left.\frac{\partial E_{PW}}{\partial V}\right|_{r_s} + \frac{dW_{PW}}{dr_s}\Big/\frac{\partial V}{\partial r_s} = \frac{2\sigma_{LG}\sin^3\theta}{r_s(2 - 3\cos\theta + \cos^3\theta)} \times\left(\frac{2}{1+\cos\theta} - \cos\theta_{EC}\right) + \frac{f(1+\cos\theta_I)\sigma_{LG}\sin^3\theta}{r_s(2 - 3\cos\theta + \cos^3\theta)} \quad (26)$$

It should be mentioned that the inner energy is not included in all of the above droplet energy calculations since the inner energy will increase equally when a droplet raises its volume through any pathway of the three modes.

Finally, the EIR of droplet system can be calculated according to eqn (11), (25) and (26) for a droplet increasing its volume through an increasing CA and enlarging base area respectively. The droplet will grow along the route with the slowest increasing energy or minimum energy barrier.

Two kinds of textured surfaces, cylindrical and squared micro/nano-pillar structures, were considered in the calculation of condensed droplet wetting morphology. If d_n and w respectively represent the diameter of cylindrical pillars and the width of squared pillars, s and h are the space and height of pillars, the Cassie–Baxter and Wenzel rough factor formulas for these two types of pillars are:[4,39,40]

$$f = \pi(d_n/s)^2/4 \quad (27)$$

$$r = 1 + \pi d_n h/s^2 \quad (28)$$

and

$$f = (w/s)^2 \quad (29)$$

$$r = 1 + 4wh/s^2 \quad (30)$$

3. Results and discussion

Since the wetting states of condensed droplets on nano-textured surfaces can be regulated by different nano-pillar geometries, the following calculations were carried out to find the effects of micro/nano parameters on the wetting evolution of condensed droplets and their final wetting states.

3.1 Energy change of condensed droplets during growth in different modes

The EIR of droplets with their volumes rising in three modes of growth are shown in Fig. 4. It can be seen from Fig. 4A that the EIR of an initial condensate spot (solid lines) in the growth mode of increasing CA is much lower than that in the other two growth patterns by enlarging the base area (dash lines) until droplet volume reaches a certain critical value, after which the difference of EIR among the three growth modes becomes too small to distinguish in the scale of this figure. Fig. 4B provides a local enlargement of Fig. 4A with a drop volume around 10^5 μm^3, which shows that $(\partial E_{SW}/\partial V)_{r_s}$ or $(\partial E_{SPW}/\partial V)_{r_s}$ is obviously higher than the corresponding other two EIRs respectively for

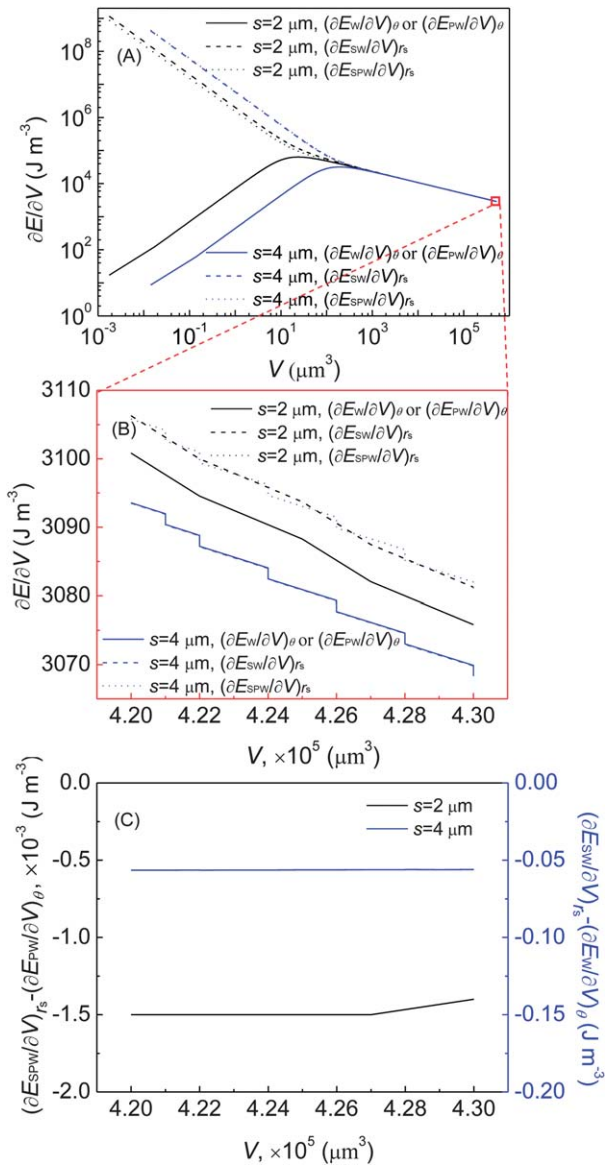

Fig. 4 Comparison of EIR of a condensed droplet with its volume growing on different textured surfaces. (A) Energy increasing rate. (B) The local enlargement of (A). (C) The differences of EIR respectively corresponding to the two marked cases in (B). $d_n = 0.3$ μm, $h = 6$ μm.

$s = 2$ μm and $s = 4$ μm. However, it is still difficult to distinguish the other two EIRs, $(\partial E_{SPW}/\partial V)_{r_s}$ and for $s = 2$ μm, as well as $(\partial E_{SW}/\partial V)_{r_s}$ and $(\partial E_W/\partial V)_\theta$ for $s = 4$ μm. To find which EIR is smallest respectively for the cases of $s = 2$ μm and $s = 4$ μm, the difference between $(\partial E_{SPW}/\partial V)_{r_s}$ and $(\partial E_{PW}/\partial V)_\theta$ as well as that between $(\partial E_{SW}/\partial V)_{r_s}$ and $(\partial E_W/\partial V)_\theta$ have to be calculated, as shown in Fig. 4C. It is thus clear that $(\partial E_{SPW}/\partial V)_{r_s}$ or $(\partial E_{SW}/\partial V)_{r_s}$ is the smallest among the EIRs of three growth modes respectively for $s = 2$ μm and $s = 4$ μm since the two differences are all negative. Therefore, condensed droplets on the textured surface with a pillar space of 2 μm will grow firstly through the mode of increasing CA and then by enlarging a composite pattern base area. *I.e.* the final fully grown condensed drops will be in a PW state. On the surface with a pillar space of 4 μm, on the other hand, the condensed drops will grow by enlarging a wetted pattern base area after growing by increasing their CA to a certain value. And the droplets will appear in a Wenzel state finally.

In general, after condensed spots form through the initial nuclei growth and coalescence within rough structures, the spots will grow firstly in the mode of increasing CA to a certain value and then in the mode of enlarging base area with the CA remaining unchanged. The wetting state of newly increased base area depends on which EIR is smaller for the two growth modes, *i.e.* droplets will enlarge their base area in the way with the slowest rise in system energy, either in a completely wetted or in a PW state, so that Wenzel droplets or PW drops will form respectively.

It is interesting to compare the dynamic behaviors of droplets during evaporation and condensation. Although the two processes are opposite, there are several similarities for the dynamic evolution of droplets. It has been well-reported that sessile droplets on super-hydrophobic surfaces can evaporate following two different modes, usually in the constant contact radius (CCR) mode first and then the constant contact angle (CCA) mode.[9,47–52] This is quite similar to the growth pattern of condensed drops on nano-textured surfaces. Namely, during the first CCR period, droplets will decrease (evaporation) or increase (condensation) their CA while keeping the base radius unchanged. On the contrary during the later CCA stage, drops will reduce (evaporation) or raise (condensation) their base radius, but with their CA almost unchanged. We think that the dynamic evolution of a droplet during evaporation also relates to its energy changing rate. The different routes a droplet follows will depend on the specific changes in the droplet's energy. The evaporation of a droplet should be along the pathway that leads to a maximum energy decrease. This needs to be the subject of further detailed studies.

3.2 Changes of droplet parameters during growth

Based on the criteria that a condensed droplet will grow in the mode with the minimum energy increase, the changes in the base radius and CA of the droplet were calculated during its

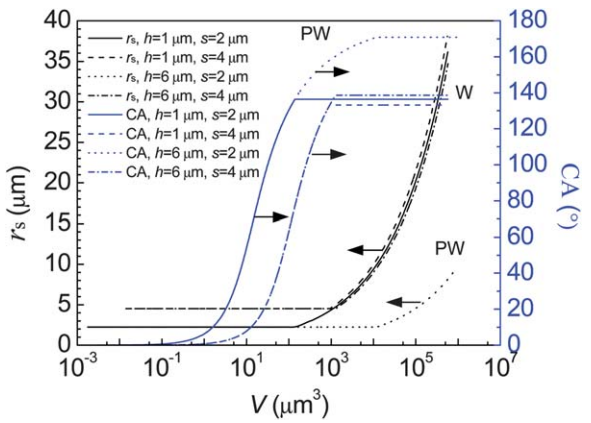

Fig. 5 Base radius and CA changes with volume as condensed droplets grow on textured surfaces with different geometric parameters.

growth on four typical nano-structured surfaces, as shown in Fig. 5. It can be seen that initially a condensed droplet grows in the CCR mode, *i.e.* with the CA increasing while with its base radius is unchanged; after the drop grows to a critical volume, its base radius begins to enlarge while its CA keeps constant, *i.e.* the CCA mode. For the cases of "$h = 1$ μm" and "$s = 2$ μm or 4 μm" for instance, the CA increases until the droplet volume reaches about 10^3 μm^3, then the CA remains constant at around 140° and r_s starts to increase. During the period of CCA, the increased area can be in a wetted state, resulting in a Wenzel droplet with its CA normally less than 160° ($h = 1$ μm and $s = 2$ μm or 4 μm; $h = 6$ μm and $s = 4$ μm);[1–15] the raised area can also be in a composite state, resulting in a PW droplet with its CA normally greater than 160° ($h = 6$ μm and $s = 2$ μm).[1,3,4] Therefore, the growth modes and state parameters of droplets all closely relate to nano-structures. When the height of the pillars is too low ($h = 1$ μm) or the space too far ($s = 4$ μm) wetted condensed droplets will form. Only when the nano-pillars have an adequate height and the space between pillars is small enough ($h = 6$ μm and $s = 2$ μm), will it be possible for condensed droplets to form in a PW state.

Both Rykaczewski *et al.*[30,34,41] and Enright *et al.*[4] observed that very small condensed drops grew in the mode of initially increasing CA then enlarging base area, which accords well with the present theoretical calculation. Rykaczewski *et al.*[30,34] also noted that the TPCL of the droplets shifted discretely during their base area enlargement, *i.e.* their CA fluctuated a little during the process, which can not be represented by our model. The CA of droplets keeps constant during the base area enlargement in our model since the two rough factors f and r were taken as constants for specific rough surface. The real local f and r however, will change when the TPCL is passed on a rough surface, that is, the local f and r are not uniform on a rough surface in a real case. Therefore, our present model can not reflect the fluctuation in the CA during the enlargement of the droplet base area. In fact, a dynamic equation is needed to describe this fluctuation of the CA. Even though our present model can only show the possible growth mode of a condensed droplet, and can not illustrate its detailed kinetic behavior, there will be a very small error for the prediction of the final wetting state of the droplet.

In addition, our calculation results also agree with those observed by Enright *et al.*[4] for the wetted state of condensed droplets on the two types of nano-textured surfaces with the same pillar diameter 300 nm and height 6.3 μm but different spaces between the pillars, 2 and 4 μm.

Furthermore, the growth of the tiny condensed droplet considered in this model is limited to the condensation of vapor on it, and does not include coalescence with other small drops, which happens under the conditions of small supersaturation and low nuclei density. On the other hand, the main pattern of droplet growth will be coalescence when supersaturation is large and nuclei density is high. In this case, tiny droplets will combine with each other easily since the distances between them are very small, so that the nano-structures can be flooded and a wetted film will form.[1,4] Our model is not valid for this latter case.

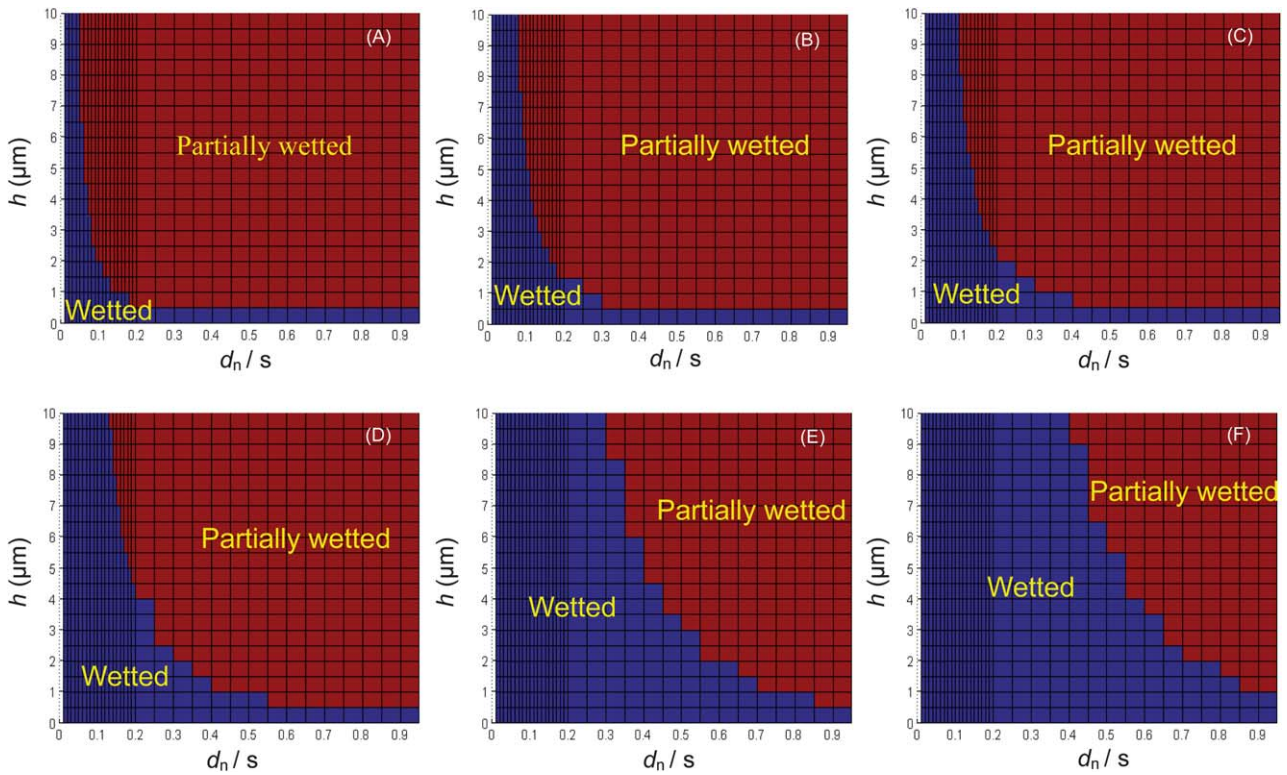

Fig. 6 Condensed droplets will appear in distinct wetting states on different textured surfaces with a wide range of nano/micro geometric parameters. (A) $d_n = 0.1$ μm; (B) $d_n = 0.3$ μm; (C) $d_n = 0.5$ μm; (D) $d_n = 1$ μm; (E) $d_n = 5$ μm; (F) $d_n = 10$ μm.

Table 1 Comparison of calculated condensed drop wetted states on nano-textured surfaces with experimental results

	Droplet wetted states				
Textured parameters	Experimental results	Calculation of this model	Formula (2)	Formula (1)	References
$\theta_I = 75°, f = 0.11, r = 1.35$	W	W	W	W	11
$\theta_I = 91°, f = 0.25, r = 7.7$	W	Cassie–Baxter/PW	Cassie–Baxter/PW	W	19
$\theta_I = 101°, f = 0.25, r = 7.7$	Cassie–Baxter/PW	Cassie–Baxter/PW	Cassie–Baxter/PW	Cassie–Baxter	19
$\theta_I = 78°, f = 0.14, r = 1.41$	W	W	W	W	14
$\theta_I = 104°, f = 0.08, r = 1.47$	W	W	W	W	14
$\theta_I = 127°, f = 0.11, r = 8.33$	Cassie–Baxter/PW	Cassie–Baxter/PW	Cassie–Baxter/PW	Cassie–Baxter	17
$\theta_I = 117°, f = 0.01, r = 7.9$	Cassie–Baxter/PW	Cassie–Baxter/PW	Cassie–Baxter/PW	Cassie–Baxter	18
$\theta_I = 90°, f = 0.01, r = 7.9$	W	Cassie–Baxter/PW	Cassie–Baxter/PW	W	18
$\theta_I = 73°, f = 0.01, r = 7.9$	W	W	W	W	18
$\theta_I = 70°, f = 0.01, r = 7.9$	W	W	Cassie–Baxter/PW	W	18
$\theta_I = 49°, f = 0.01, r = 7.9$	W	W	Cassie–Baxter/PW	W	18
$\theta_I = 103.2°, f = 0.018, r = 3.26$	Cassie–Baxter/PW	Cassie–Baxter/PW	Cassie–Baxter/PW	W	4
$\theta_I = 103.2°, f = 0.004, r = 1.56$	W	W	W	W	4
$\theta_I = 101°, f = 0.06, r = 8.9$	Cassie–Baxter/PW	Cassie–Baxter/PW	Cassie–Baxter/PW	Cassie–Baxter	4
$\theta_I = 101°, f = 0.11, r = 1.15$	W	W	W	W	4
$\theta_I = 101°, f = 0.11, r = 1.3$	W	W	W	W	4
$\theta_I = 101°, f = 0.11, r = 1.55$	W	W	W	W	4
$\theta_I = 101°, f = 0.11, r = 1.6$	W	W	W	W	4
$\theta_I = 101°, f = 0.11, r = 1.76$	Cassie–Baxter/PW	Cassie–Baxter/PW	W	W	4
$\theta_I = 101°, f = 0.11, r = 1.78$	Cassie–Baxter/PW	Cassie–Baxter/PW	W	W	4
$\theta_I = 101°, f = 0.11, r = 2.11$	Cassie–Baxter/PW	Cassie–Baxter/PW	Cassie–Baxter/PW	W	4
$\theta_I = 101°, f = 0.11, r = 2.43$	Cassie–Baxter/PW	Cassie–Baxter/PW	Cassie–Baxter/PW	W	4
$\theta_I = 101°, f = 0.11, r = 3.17$	Cassie–Baxter/PW	Cassie–Baxter/PW	Cassie–Baxter/PW	W	4
$\theta_I = 101°, f = 0.11, r = 3.57$	Cassie–Baxter/PW	Cassie–Baxter/PW	Cassie–Baxter/PW	W	4
$\theta_I = 101°, f = 0.11, r = 5.05$	Cassie–Baxter/PW	Cassie–Baxter/PW	Cassie–Baxter/PW	Cassie–Baxter	4
$\theta_I = 101°, f = 0.11, r = 8.24$	Cassie–Baxter/PW	Cassie–Baxter/PW	Cassie–Baxter/PW	Cassie–Baxter	4
$\theta_I = 113.5°, f = 0.1, r = 2.97$	Cassie–Baxter/PW	Cassie–Baxter/PW	Cassie–Baxter/PW	Cassie–Baxter	4
$\theta_I = 101°, f = 0.023, r = 10$	Cassie–Baxter/PW	Cassie–Baxter/PW	Cassie–Baxter/PW	Cassie–Baxter	1

3.3 Wetted states of condensed droplets on rough surfaces and the relation with structural parameters

Fig. 6 illustrates the influence of nano-structural parameters on the wetting states of condensed droplets in more detail. It can be seen that height of micro/nano-pillars above 1 μm is one of the necessary conditions for condensed droplets in the PW state. The smaller the diameter and pitch between pillars, the easier it is for the drops to form in a PW state. Specially, when the diameter of the pillars is beyond 10 μm, the region for droplets in a PW state becomes small, in which case a larger ratio of diameter and space, d_n/s, is needed. Generally, a droplet will easily appear in a PW state on a surface with a high h and small s since the energy of completely wetted droplets is high in this case.

The experimental observation and model calculation results are summarized in Tables 1 and 2 for the wetted states of condensed droplets on nano- and micro-textured surfaces respectively. It can be found from Table 1 that most of the

Table 2 Comparison of calculated condensed drop wetted states on micro-textured surfaces with experimental results

	Droplet wetted states				
Textured parameters	Experimental results	Calculation of this model	Formula (2)	Formula (1)	References
$\theta_I = 118°, f = 0.25, r = 6$	Wenzel + Cassie–Baxter	Cassie–Baxter/PW	Cassie–Baxter/PW	Cassie–Baxter	53
$\theta_I = 118°, f = 0.11, r = 5.4$	Wenzel + Cassie–Baxter	Cassie–Baxter/PW	Cassie–Baxter/PW	Cassie–Baxter	53
$\theta_I = 95°, f = 0.04, r = 1.64$	W	W	W	W	5
$\theta_I = 90°, f = 0.25, r = 2.94$	W	Cassie–Baxter/PW	Cassie–Baxter/PW	W	6
$\theta_I = 110°, f = 0.0625, r = 2.25$	W	Cassie–Baxter/PW	Cassie–Baxter/PW	W	8
$\theta_I = 98°, f = 0.13, r = 2.0$	W	Cassie–Baxter/PW	Cassie–Baxter/PW	W	9
$\theta_I = 98°, f = 0.23, r = 2.95$	W	Cassie–Baxter/PW	Cassie–Baxter/PW	W	9
$\theta_I = 117.3°, f = 0.4, r = 4.05$	Wenzel + Cassie–Baxter	Cassie–Baxter/PW	Cassie–Baxter/PW	Cassie–Baxter	12
$\theta_I = 101°, f = 0.19, r = 1.8$	W	Cassie–Baxter/PW	Cassie–Baxter/PW	W	19
$\theta_I = 101°, f = 0.095, r = 1.82$	W	Cassie–Baxter/PW	Cassie–Baxter/PW	W	19
$\theta_I = 91°, f = 0.19, r = 1.8$	W	Cassie–Baxter/PW	W	W	19
$\theta_I = 91°, f = 0.095, r = 1.82$	W	W	W	W	19

calculated results of this model are consistent with those of experiments, with the accuracy of 91.9%, while the accuracies of calculations with the formulas (1) and (2) are only 75% and 78.6% respectively. On the other hand, it can be seen from Table 2 that the calculation results of this model are not well in agreement with experiments for condensed drops on surfaces with micro structures. The accuracy of this model is only about 41.7% in this case. And the accuracy of formula (2) is also low, 50%. However, the accuracy of formula (1) is almost 100% in this case, which indicates that the condensed drops in the micro-textured surfaces are more likely to be approaching towards an equilibrium state so that their wetted states are consistent with the calculation of formula (1).

Because the space between micro-pillars is much larger than that between nano-pillars, the ratio of the distance L between the condensate nuclei and the space s of the micro-pillars, L/s, is small. Therefore, the adjacent drops in micro-structures are closer to each other and more easily merge, resulting in the final droplets being in a wetted state. It has been reported by Enright *et al.*[4] that condensed droplets on textured surfaces when L/s is less than 3 will appear in a wetted state because of the coalescence. It is difficult for L/s to be greater than 3 for condensation on micro-structured surfaces while L/s on nano-textured surfaces can be larger than 3 since the space between the nano-pillars is much smaller. Therefore, PW droplets can form on nano-textured surfaces under low supersaturation.

Condensed droplets on the current nano-textured surfaces appeared in a PW state only under low supersaturation.[1–3] And such drops after coalescence could jump and shift away from the surfaces[1–3,20,21,27,54,55] so that efficient dropwise condensation may be realized.[1] However, once the supersaturation is large, the condensed droplets on the present textured surfaces will quickly merge and flood the nano-structures,[1] which leads to wetted droplets or even filmwise condensation.[36,56] How to avoid the flooding of nano-textures is one of the key issues to consider in the design and preparation of novel super-hydrophobic textured surfaces.

4. Conclusions

The minimum EIR can be used to determine the growth modes and wetting states of condensed droplets on nano-textured surfaces. Although there are three growth routes for condensed droplets on textured surfaces, the EIR of droplets corresponding to each mode is different, and condensed drops will grow through the mode with the minimum energy increase, usually increasing their CA firstly, and then enlarging their base area. Moreover, the growth modes of condensed droplets are dependent on nano-textured parameters. Completely wetting drops will form on the surfaces with low pillar heights and/or large spaces between pillars. And PW drops can only form on surfaces with a pillar height higher than 1 μm and with a relatively small pillar diameter and space. These findings may be useful in the design of super-hydrophobic surfaces enabling droplet shedding early and quickly to sustain efficient super-hydrophobicity for condensation.

Acknowledgements

The authors acknowledge financial support from the National Natural Science Foundation of China (no. 50876015).

Notes and references

1 N. Miljkovic, R. Enright, Y. Nam, K. Lopez, N. Dou, J. Sack and E. N. Wang, *Nano Lett.*, 2013, **13**, 179–187.
2 K. Rykaczewski, A. T. Paxson, S. Anand, X. Chen, Z. Wang and K. K. Varanasi, *Langmuir*, 2013, **29**, 881–891.
3 N. Miljkovic, R. Enright and E. N. Wang, *ACS Nano*, 2012, **6**, 1776–1785.
4 R. Enright, N. Miljkovic, A. Al-Obeidi, C. V. Thompson and E. N. Wang, *Langmuir*, 2012, **28**, 14424–14432.
5 R. D. Narhe and D. A. Beysens, *Europhys. Lett.*, 2006, **75**, 98–104.
6 R. D. Narhe and D. A. Beysens, *Langmuir*, 2007, **23**, 6486–6489.
7 R. D. Narhe and D. A. Beysens, *Phys. Rev. Lett.*, 2004, **93**, 076103.
8 K. A. Wier and T. J. McCarthy, *Langmuir*, 2006, **22**, 2433–2436.
9 Y. C. Jung and B. Bhushan, *J. Microsc.*, 2008, **229**, 127–140.
10 A. Lafuma and D. Quere, *Nat. Mater.*, 2003, **2**, 457–460.
11 R. D. Narhe, W. Gonzalez-Vinas and D. A. Beysens, *Appl. Surf. Sci.*, 2010, **256**, 4930–4933.
12 X. L. Chen and T. Lu, *Sci. China, Ser. G: Phys., Mech. Astron.*, 2009, **52**, 233–238.
13 X. Xiao, Y. T. Cheng, B. W. Sheldon and J. Rankin, *J. Mater. Res.*, 2008, **23**, 2174–2178.
14 T. Furuta, M. Sakai, T. Isobe and A. Nakajima, *Langmuir*, 2010, **26**, 13305–13309.
15 C. Dietz, K. Rykaczewski, A. Fedorov and Y. Joshi, *J. Heat Transfer*, 2010, **132**, 080904.
16 S. A. Kulinich, S. Farhadi, K. Nose and X. W. Du, *Langmuir*, 2011, **27**, 25–29.
17 K. K. S. Lau, J. Bico, K. B. K. Teo, M. Chhowalla, G. A. J. Amaratunga, W. I. Milne, G. H. McKinley and K. K. Gleason, *Nano Lett.*, 2003, **3**, 1701–1705.
18 C. Dorrer and J. Ruehe, *Adv. Mater.*, 2008, **20**, 159–163.
19 C. H. Chen, Q. J. Cai, C. L. Tsai, C. L. Chen, G. Y. Xiong, Y. Yu and Z. F. Ren, *Appl. Phys. Lett.*, 2007, **90**, 173108.
20 J. B. Boreyko and C. H. Chen, *Phys. Rev. Lett.*, 2009, **103**, 184501.
21 J. B. Boreyko and C. H. Chen, *Phys. Fluids*, 2010, **22**, 091110.
22 X. M. Chen, J. Wu, R. Y. Ma, M. Hua, N. Koratkar, S. H. Yao and Z. K. Wang, *Adv. Funct. Mater.*, 2011, **21**, 4617–4623.
23 C. Dietz, K. Rykaczewski, A. G. Fedorov and Y. Joshi, *Appl. Phys. Lett.*, 2010, **97**, 033104.
24 K. K. Varanasi, M. Hsu, N. Bhate, W. Yang and T. Deng, *Appl. Phys. Lett.*, 2009, **95**, 094101.
25 L. Y. Huang, Z. L. Liu, Y. M. Liu and Y. J. Gou, *Int. J. Therm. Sci.*, 2011, **50**, 432–439.
26 M. He, J. J. Wang, H. L. Li and Y. L. Song, *Soft Matter*, 2011, **7**, 3993–4000.

27 M. He, X. Zhou, X. P. Zeng, D. P. Cui, Q. L. Zhang, J. Chen, H. L. Li, J. J. Wang, Z. X. Cao, Y. L. Song and L. Jiang, *Soft Matter*, 2012, **8**, 6680–6683.
28 J. Feng, Z. Q. Qin and S. H. Yao, *Langmuir*, 2012, **28**, 6067–6075.
29 T. J. Ko, E. K. Her, B. Shin, H. Y. Kim, K. R. Lee, B. K. Hong, S. H. Kim, K. H. Oh and M. W. Moon, *Carbon*, 2012, **50**, 5085–5092.
30 K. Rykaczewski, W. A. Osborn, J. Chinn, M. L. Walker, J. H. J. Scott, W. Jones, C. L. Hao, S. H. Yao and Z. K. Wang, *Soft Matter*, 2012, **8**, 8786–8794.
31 T. S. Yu, J. Park, H. Lim and K. S. Breuer, *Langmuir*, 2012, **28**, 12771–12778.
32 Q. L. Zhang, M. He, X. P. Zeng, K. Y. Li, D. P. Cui, J. Chen, J. J. Wang, Y. L. Song and L. Jiang, *Soft Matter*, 2012, **8**, 8285–8288.
33 J. Feng, Y. C. Pang, Z. Q. Qin, R. Y. Ma and S. H. Yao, *ACS Appl. Mater. Interfaces*, 2012, **4**, 6618–6625.
34 K. Rykaczewski, *Langmuir*, 2012, **28**, 7720–7729.
35 K. Rykaczewski, T. Landin, M. L. Walker, J. H. J. Scott and K. K. Varanasi, *ACS Nano*, 2012, **6**, 9326–9334.
36 J. T. Cheng, A. Vandadi and C. L. Chen, *Appl. Phys. Lett.*, 2012, **101**, 131909.
37 S. Anand, A. T. Paxson, R. Dhiman, J. D. Smith and K. K. Varanasi, *ACS Nano*, 2012, **6**, 10122–10129.
38 B. S. Shin, K. R. Lee, M. W. Moon and H. Y. Kim, *Soft Matter*, 2012, **8**, 1817–1823.
39 T. Q. Liu, W. Sun, X. Y. Sun and H. R. Ai, *Langmuir*, 2010, **26**, 14835–14841.
40 T. Q. Liu, W. Sun, X. Y. Sun and H. R. Ai, *Acta Phys.-Chim. Sin.*, 2010, **26**, 2989–2996.
41 K. Rykaczewski and J. H. J. Scott, *ACS Nano*, 2011, **5**, 5962–5968.
42 F. C. Wang, F. Q. Yang and Y. P. Zhao, *Appl. Phys. Lett.*, 2011, **98**, 053112.
43 J. W. Harris and H. Stocker, *Handbook of Mathematics and Computational Science*, Springer-Verlag, New York, 1998, p. 107.
44 C. T. Hsieh, F. L. Wu and W. Y. Chen, *J. Phys. Chem. C*, 2009, **113**, 13683–13688.
45 S. D. Iliev, *J. Colloid Interface Sci.*, 1997, **194**, 287–300.
46 C. Andrieu, C. Sykes and F. Brochard, *Langmuir*, 1994, **10**, 2077–2080.
47 W. Xu, R. Leeladhar, Y. T. Kang and C. H. Choi, *Langmuir*, 2013, **29**, 6032–6041.
48 K. R. Khedir, G. K. Kannarpady, H. Ishihara, J. Woo, S. Trigwell, C. Ryerson and A. S. Biris, *J. Phys. Chem. C*, 2011, **115**, 13804–13812.
49 H. Gelderblom, A. G. Marin, H. Nair, A. van Houselt, L. Lefferts, J. H. Snoeijer and D. Lohse, *Phys. Rev. E: Stat., Nonlinear, Soft Matter Phys.*, 2011, **83**, 026306.
50 X. M. Chen, R. Y. Ma, J. T. Li, C. L. Hao, W. Guo, B. L. Luk, S. C. Li, S. H. Yao and Z. K. Wang, *Phys. Rev. Lett.*, 2012, **109**, 116101.
51 C. H. Choi and C. J. Kim, *Langmuir*, 2009, **25**, 7561–7567.
52 X. Y. Zhang, S. X. Tan, N. Zhao, X. L. Guo, X. L. Zhang, Y. J. Zhang and J. Xu, *ChemPhysChem*, 2006, **7**, 2067–2070.
53 C. Dorrer and J. Ruehe, *Langmuir*, 2007, **23**, 3820–3824.
54 T. Q. Liu, W. Sun, X. Y. Sun and H. R. Ai, *Colloids Surf., A*, 2012, **414**, 366–374.
55 T. Q. Liu, W. Sun, X. Y. Sun and H. R. Ai, *Acta Phys.-Chim. Sin.*, 2012, **28**, 1206–1212.
56 D. Torresin, M. K. Tiwari, D. Del Col and D. Poulikakos, *Langmuir*, 2013, **29**, 840–848.